Journal of Molecular Catalysis B: Enzymatic 108 (2014) 43–50

Contents lists available at ScienceDirect

Journal of Molecular Catalysis B: Enzymatic

journal homepage: www.elsevier.com/locate/molcatb

Stabilization of *Candida rugosa* lipase on nanosized zirconia-based materials

Maya Guncheva*, Krasimira Paunova, Momtchil Dimitrov, Denitsa Yancheva

Institute of Organic Chemistry with Centre of Phytochemistry, Bulgarian Academy of Sciences, 1113 Sofia, Bulgaria

ARTICLE INFO

Article history:
Received 25 April 2014
Received in revised form 28 June 2014
Accepted 29 June 2014
Available online 8 July 2014

Keywords:
Candida rugosa lipase
Nanosized zirconia-based materials
Enzyme stabilization
Enantioselectivity

ABSTRACT

We synthesized and characterized three novel materials on the basis of zirconia. Despite their three-to six fold higher specific surface area, nanoZrO_2-CeO_2 (150 m^2/g) and nanoZrO_2-B (296 m^2/g) they proved to be less effective supports for a lipase from *Candida rugosa* than nanoZrO_2-A. For the last, we achieved protein loading of 23 mg/g, distributed in a monolayer, which means that 61% of the carrier surface was occupied by the protein. The immobilized on nanoZrO_2-A lipase (nanoZrO_2-A-CRL) exhibited enhanced thermal and solvent stability in comparison to the native enzyme. NanoZrO_2-A-CRL has a half-life at 55 °C of 73 min, while for the native enzyme it was only 5.3 min. The immobilized enzyme preserved 20% of its activity in six consecutive cycles of the reaction hydrolysis of tributyrin. The immobilization influenced the enantioselectivity of CRL. Using nanoZrO_2-A-CRL under optimal reaction condition in the reaction of esterification of lauric acid with (±)-menthol, we achieved menthol conversion of 43% (*i.e.* 82% of (−) methyl laurate), enantiomeric excess of 97% and enantiomeric ratio of 144. The conformational analysis proved that upon immobilization no serious change in the secondary structure of the lipase from *Candida rugosa* had occurred.

1. Introduction

Lipases (EC 3.1.1.3) are large group of enzymes that in aqueous media catalyze the hydrolysis of ester-bonds in triglyceride substrates to glycerol and free fatty acids. In non-aqueous media they can catalyze the reverse reaction, *i.e.* the reaction of esterification [1]. All lipases belong to "α/δ-hydrolase fold" family and most of them have a highly conservative pentapeptide sequence (Gly-X-Ser-X-Gly) that includes the active nucleophile serine residue [2]. The active site of lipases consists of three amino acid residues (serine, histidine, aspartate or glutamate) known as "catalytic triad". These enzymes share a common mechanism which includes steps of acylation and deacylation. During each step acyl-enzyme and tetrahedral intermediate are formed, the latter is stabilized by the amino acid residues assembling the "oxyanion hole" [3]. Another structural and mechanistic feature typical for most of the lipases is the presence of α-helical fragment ("lid") which covers the active site in absence of substrate and protect the enzyme. Upon contact with the hydrophobic substrates or organic solvents the "lid" undergoes a conformational change, moves away and the active site of the enzyme becomes accessible to the reagents. This phenomenon is known as "interfacial activation" [4]. Similar activation upon binding to hydrophobic surfaces has been observed for many lipases. For example, Palomo et al. reported enhanced thermal and solvent stability as well as hyperactivation of the immobilized on octadecyl-sepabeads lipase from Bacillus thermocatenulatus with respect to the soluble enzyme [5]. The same interfacial hyperactivation by physical adsorption on hydrophobisized vinyl-based amphiphilic polymers was reported for the lipase from *Candida rugosa* [6] and for many other lipases from various species (*Candida antarctica*, *Humicola lanuginosa*, *Mucor javanicus*, *Rhizomucor miehei*, *Pseudomonas fluorescens*, *Rhizopus niveus*) when immobilized on octyl-agarosa [7].

Lipases are enzymes of considerable industrial significance. They are widely applied in food, detergent, pharmaceutical and cosmetic industries as well as in paper, textile and leather processing [8]. Yet, their price is high in comparison with chemical catalysts and their utilization in several consecutive cycles is envisaged. Use of immobilized enzymes has many advantages over the soluble enzymes. They can be easily separated from the reaction mixture *i.e.* the reaction can be easily terminated, immobilized enzymes usually are more stable at higher temperatures and organic solvents, as well as they can be used several operation cycles [9].

Nanobiotechnology is a new fast developing trend of biotechnology. It has shown great potential in applications such as: biosensing,

* Corresponding author. Tel.: +359 29606160; fax: +359 28700225.
E-mail address: maiag@orgchm.bas.bg (M. Guncheva).

http://dx.doi.org/10.1016/j.molcatb.2014.06.012
1381-1177/

drug delivery, protein immobilization, and many others. Excellent enzyme stabilization upon immobilization on various nanomaterials (nanoparticles, nonofibres, nanopubes, nanopores, nanosheets and nanocoposites) has been reported and is the basis for the development of a new sub-field in biocatalysis, *i.e.* nanobiocatalysis [10,11]. In addition, systems with trapped in nanospaces several enzymes are good model for studying the protein-protein interactions inside the cells which still are not completely elucidated. For example, *in vivo* many enzymes are located in the organelles and they are catalytically active under crowded environment, however, *in vitro* most of enzymes are prone to easy aggregation and unfolding even at concentrations of 1 mg/mL. Within the aggregates, the enzyme active centre remains inaccessible to the substrate molecules and usually low activity is detected under such conditions. In some cases, the addition of small quantities of non-ionic surfactants to the enzyme solutions can be beneficial and prevent aggregation. Another successful strategy for protein stabilization is immobilization, especially on nanosized particles [12].

Inorganic nanostructures are characterized with large surface area, narrow particle size distribution, mechanical strength and resistance to microbial attack and organic solvents. In addition, they can be well-dispersed in liquid reaction media and thus the problem with low protein solubility in organic medium is overcome as well as good homogenization of the reaction mixture can be achieved [13]. Biocompatible particles on the basis of silica, iron oxides, carbon (grapheme, diamond), gold, *etc.* have been obtained in nanosize dimensions. Their surface and pore size can be easily modified by functionalization or/and coating with organic compounds which makes them applicable for immobilization and stabilization of various proteins and enzymes.

Zirconia is a polymorphic bioinert material that possesses the above discussed favourable characteristics of the inorganic materials such as: high thermal, pH- and solvent stability, *etc.* It occurs in three temperature-depending forms: monoclinic, tetragonal and cubic. There are several papers on application of zirconium dioxide in chromatography, preparation of enzyme-based reactors and biosensors. There are also reports on the utilization of zirconia nanoparticles as enzyme carriers. For example, the α-amylase form *Bacillus subtilis* immobilized on zirconia exhibited good stability and activity in the reaction of hydrolysis of starch [14]. Bellezza et al. reported on excellent catalytic efficiency of the myoglobin immobilized on phosphoric acid (or benzenephosphonic acid) grafted zirconia [15]. There is also a report on the selective adsorption of different isoforms of *C. rugosa* lipase on α-zirconium phosphate and phosphonates and an enhanced enantioselectivity of the immobilized lipase preparations in the reaction of hydrolysis of (±)-methyl-2-(4-chlorophenoxy) propionate [16]. We think that the results on zirconia-based biocatalysts found in the literature are very attractive but that the potential of zirconia as nanocarrier is not fully revealed and worth further investigations.

We synthesized and characterized three materials based on zirconia. They were tested as suitable supports for a lipase from *C. rugosa*. The lipase from the yeast *C. rugosa* is a glycoprotein that presents in different isoforms and isoenzymes which differ in their stability and specificity [17]. It is widely used for industrial production of highly pure unsaturated fatty acids, synthesis or kinetic resolution of racemic mixture of some therapeutics, synthesis of flavour esters for food and perfume industries, in detergent formulations, *etc.* [18].

We assessed the effect of surface morphology, particle and pore sizes and surface area of the carriers on their lipase loading capacity. The catalytic efficiency of the two promising immobilized enzymes was estimated in a hydrolytic reaction. Then, their thermo-, solvent, and operational stability was estimated. The novel most stable and active catalyst was tested in a reaction of enantioselective acylation of (±)-menthol.

2. Materials and methods

2.1. Materials

Lipase from *C. rugosa* (CRL) (MW 64 kDa, 30 U/mg (olive oil as substrate), 20% (w/w) protein content) was provided by Amano Pharmaceutical Co., Japan. Glyceryl tributyrate (99% purity), Folin & Ciocalteu's phenol reagent (2 N, suitable for determination of total protein by Lowry's method) were purchased from Sigma, Germany. Lauric acid (>98%), (±)-menthol (98%), (1R, 2S, 5R) (−)-menthol (99%), (1S, 2R, 5S)(+)-menthol (99%), zirconium (IV) chloride (>99.9% purity), cerium(III) chloride heptahydrate (99.9%) and hexadecyl-N,N,N-trimethylammoniumbromide (CTAB) were obtained from Sigma–Aldrich, Germany.

2.2. Synthesis of the nanosized ZrO_2-A, ZrO2-B and ZrO_2-CeO_2

For the synthesis of the nanostructured zirconia samples a template-assisted approach was used following a procedure reported by Tsoncheva et al. [19]. In principle, 12.0 g N-hexadecyl-N,N,N-trimethylammoniumbromide (CTAB) were dissolved in 100 mL distilled water. To this solution was added slowly and under vigorous stirring a second solution of $ZrCl_4$ (6.80 g) in 50 mL distilled water. In the case of the mixed oxide sample the second solution contained a mixture of $ZrCl_4$ (3.40 g) and $CeCl_3 7H_2O$ (5.40 g) in 50 mL distilled water. Then, the temperature was raised to 50 °C and the reaction mixture was stirred for 30 min before adding dropwise 40 mL NH_4OH (12.5%). The resulting mixture was stirred overnight at 50 °C. Then it was transferred into a polypropylene container and treated at 100 °C for 24 h. The so-prepared particles were then filtrated, washed with distilled water, then dried at room temperature and calcinated up to 300 °C (nanoZrO_2-B and nanoZrO_2-CeO_2) or 500 °C (nanoZrO_2-A) with a ramp of 1 °C/min and dwelling time of 15 h at the final temperature. For, nanoZrO_2-A the hydrothermal treatment step was skipped and an extraction of the organic template in absolute ethanol (100 mL per 1 g carrier) was conducted at 70 °C for 24 h. Then, the sample was filtrated and dried at room temperature before calcination.

2.3. Characterization of the particles

Powder X-ray diffraction patterns were collected within the range of 10–80° 2θ with a constant step of 0.02° 2θ and counting time of 1 s/step on Bruker D8 Advance diffractometer equipped with Cu Kα radiation and LynxEye detector. The size of the crystalline domains in the samples was determined using Topas 4.2 software with Rietveld quantification refinement for nanoZrO_2-A, and the Scherrer equation [20] in case of the other samples. Nitrogen sorption measurements were recorded on a Quantachrome NOVA 1200e instrument at 77 K. Before the physisorption measurements the samples were outgassed at 423 K overnight under vacuum.

2.4. Immobilization of lipase from Candida rugosa

In a typical preparation, 20 mg of carrier (nanoZrO_2-A, nanoZrO_2-B, nanoZrO_2-CeO_2) was mixed and was gently stirred with 5.0 mL solution of *C. rugosa* lipase (CRL) for 12 h at room temperature and then incubated overnight at 4 °C. The protein concentration in the loading solutions (50 mM sodium phosphate buffer, pH 7.0) was in the range 0.05–1 mg/mL. After the incubation, the immobilized biocatalysts were filtered and freeze-dried.

2.5. Protein assay

The amount of the protein in the lipase loading solutions and in the supernatant after immobilization was estimated according to Lowry et al. using bovine albumin as standard [21].

The amount of the protein attached to the carrier (mg protein/g support) was calculated by the following equation:

$$Q_e = \frac{V(C_0 - C_e)}{m},$$

where C_0 and C_e (mg/mL) are the initial and the final protein concentration of the lipase loading solutions, respectively, V (mL) is the volume of the enzyme solution, m (g) is the quantity of the support. The Langmuir and Freundlich constants were calculated as described in the literature [22].

2.6. Infrared spectroscopy

FTIR spectra of the supports, the native and the immobilized lipase from *C. rugosa* were recorded using Bruker Tensor 27 spectrometer, equipped with a detector of deuterated triglycine sulphate (DTGS). The FTIR spectra were collected by direct deposition of the samples on attenuated total reflectance (ATR) element (diamond crystal) and in pellets of KBr at room temperature. The FTIR spectra were collected in frequency region 4000–700 cm^{-1} (ATR) and 4000–400 cm^{-1}, (KBr) with 128 scanning and at resolution of 2 cm^{-1}. The ATR-FTIR spectrum of the native CRL was rationed against the background air spectrum. The ATR-FTIR spectra of the immobilized CRL were referenced to the respective supports in order to substact their absorptions.

In order to describe quantitatively the changes in the enzyme secondary structure due to the immobilization, the ATR-FTIR spectra were treated in accordance with the established methods given in the literature [23,24].

ATR-FTIR spectra were Fourier deconvoluted by Opus software version 5.5 using band width of 14 cm^{-1}, 2.9 resolution enhancement factor, and Lorentzian lineshape. Second derivative spectra were obtained using the Savitzky–Golay algorithm based on 13 smoothing points. Then, the relative contribution of each band component of the Amide I band was determined by curve fitting following the procedure of OPUS programme. In the fitting, the number of components and the initial values of their position were set as determined from the second derivative spectra. The initial bandwidth of all components was set to 14 cm^{-1} and the components were approximated by mixed Lorentzian/Gaussian functions. The curve-fitting was performed according to the Local Least Squares algorithm.

2.7. Hydrolytic activity of the immobilized biocatalysts

The hydrolytic activity of the free and the immobilized lipase preparations was estimated titrimetrically using 0.05 M sodium hydroxide as titrant. All experiments were performed at 40 °C for 30 min at stirring rate of 200 rpm. The reaction mixture contained 0.1 mL tributyrin, 0.1 mL gum arabica (5 mg/mL stock solution), 5 mL sodium phosphate buffer (50 mM, pH 7.5) and 5 mg immobilized enzyme preparation (or 50 μL free lipase with concentration of 1 mg/mL). Control experiments under the same reaction conditions without added enzyme were run in order to take into account the spontaneous hydrolysis.

One lipase unit (U) is defined as the amount of enzyme required to liberate 1 μmol butyric acid per min under the assay conditions. The activity of the immobilized lipase preparations is presented as the number of lipase units per gram support (U/g carrier). The specific activity corresponds to the number of lipase units per mg of protein (U/mg prot.).

To test the operational stability of the immobilized biocatalysts, prior to use in the next cycle the biocatalyst was isolated from the reaction mixture by filtration and washed with two portion of 0.5 mL hexane. The activity of the biocatalysts in the first cycle was taken for 100%.

2.8. Thermal and solvent stability of the immobilized lipases

To test the thermal stability of the novel biocatalysts in comparison with the native enzyme, the soluble and the immobilized lipases were incubated in presence of 50 mM sodium phosphate buffer (pH 7.0) at 55 °C for different time intervals. Then, the residual activity of the thermally treated biocatalysts was assessed in a reaction of hydrolysis of tributyrin as described above. The half-life time was calculated according to the following equations [25]:

$$\alpha = \frac{E}{E_0} = e^{-kdt} \text{ and } t_{1/2} = \frac{\ln 2}{k_d}$$

where α is deactivation, E and E_0 are the specific activities of the biocatalysts in (U/mg) at given and zero times, k_d deactivation constant. The slope in the plot of $\ln(\alpha)$ *vs* time gives the deactivation constant (k_d).

The stability of the immobilized preparations in organic solvents was tested as follows: 10 mg immobilized lipase were incubated for 1 h with 1 mL of various water miscible or immiscible solvents (alcohols, ethers, hydrocarbons) at room temperature. Then, their activity was tested in reaction of hydrolysis of tributyrin as described in Section 2.7. The activity of the biocatalysts in each organic solvent was compared to the activity of the non-treated enzyme which was taken for 100%.

2.9. Enzymatic acylation of (±)-menthol

In a typical experiment, 0.4 mmol of (±)-menthol and 5 U biocatalyst (20 mg immobilized or appropriate amount of native CRL) were gently stirred with 1 mL organic solvent in a thermostated at 25 °C screw-capped vial. The reaction was initiated by adding 0.4 mmol acylating reagent (lauric acid or methyl laurate). The initial water activity of the reaction mixture was maintained at 0.33 by using saturated solution of magnesium chloride [26], and then maintained using molecular sieve 3 Å. Control experiments without enzyme were performed. To determine the temperature effect on the efficiency and enantioselectivity of both studied biocatalysts, the reactions of acylation were performed in the temperature range from 20 °C to 40 °C.

Aliquots (100 μL) from the reaction mixture were withdrawn periodically, extracted with 500 μL of hexane/5%$NaHCO_3$ (1:1), and the hexane layer was analyzed by gas chromatography. The analyses were performed on a Shimadzu GC-17A instrument equipped with CycloSil-B (Agilent) column (0.25 μm × 0.25 mm × 30 m) and fitted with a flame ionization detector. The column was maintained at 90 °C for 10 min, and then the temperature was increased first to 150 °C at 3 °C/min, and after that to 165 °C at 5 °C/min, and finally the temperature was maintained at 165 °C for 5 min. The temperature of the injector was 220 °C and that of the detector–250 °C. Nitrogen was used as a gas carrier. The retention times were 24.3 min for (+)-menthol, 25.1 min for (−)-menthol.

The conversion in percentage was calculated from the following equation:

$$c = \left(1 - \frac{S}{S_0}\right) \times 100,$$

where S_0 and S stand for the concentration of (±)-menthol at the beginning and at the end of the reaction, respectively.

The enantioselectivity for each reaction was expressed by enantiomeric excess (e.e.(P_-)) and enantiomeric ratio (E-value), which

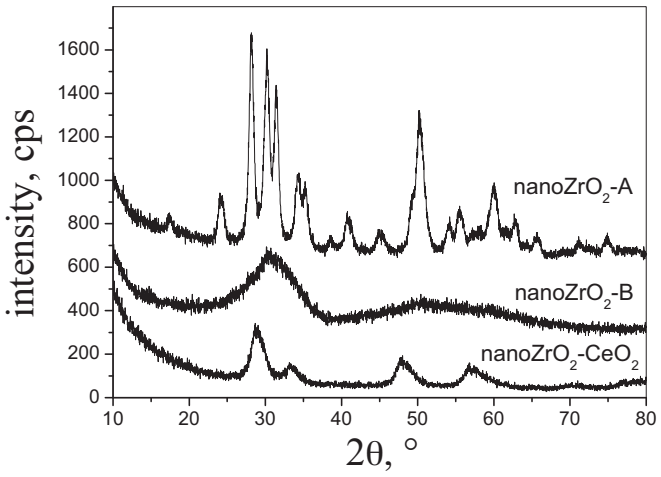

Fig. 1. X-ray diffraction patterns of zirconia and mixed zirconia-ceria samples.

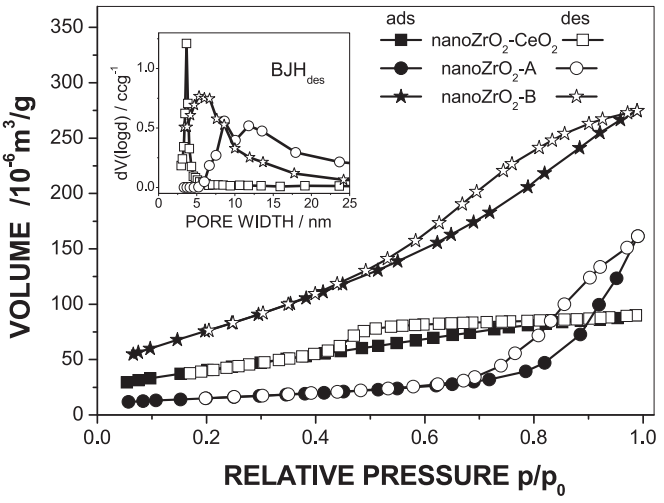

Fig. 2. Nitrogen physisorption isotherms of the studied zirconia and mixed zirconia-ceria samples with BJH pore size distributions as inset.

was calculated using the equation given by Straathof and Jongejan [27].

$$e.e.(P_-)(\%) = \frac{P_-^- P_+}{P_-^+ P_+}.100$$

$$E = \frac{\ln(1 - c(1 + e.e.P_-))}{\ln(1 - c(1 - e.e.P_-))},$$

where P_- and P_+ represent the ratios of (−)-methyl acetate and (+)-methyl acetate to total methyl acetate, respectively

2.10. Statistical analysis

All experiments were done in triplicate: the value reported refers to means. Standard deviation was determined using Microsoft Excel.

3. Results and discussion

3.1. Characterization of the synthesized nanostructured zirconia and mixed ceria-zirconia samples

We synthesized three nanosized materials–pure zirconia (nanoZrO_2-A and nanoZrO_2-B) and mixed ceria-zirconia (nanoZrO_2-CeO_2). The X-ray diffraction patterns showed that nanoZrO_2-A sample is a mixture of monoclinic (78%) and tetragonal (22%) zirconia phases consisting of well-crystalline particles with sizes of about 13 nm (Fig. 1). In contrast, nanoZrO_2-B displays very broad reflections that can be assigned to the presence of small zirconia clusters with parameters of tetragonal zirconia phase. In this case we can not talk about well-crystalline particles as their size is only about 1 nm and it is more correct to assume this material as amorphous. In case of the mixed cerium-zirconia oxide sample (nanoZrO_2-CeO_2), broad and asymmetric reflections are registered due to the superposition of very finely dispersed ceria and zirconia particles with average size of about 5 nm (Fig. 1, Table 1). The nitrogen physisorption measurements of the studied materials are quite different (Fig. 2). The highest specific surface area and total pore volume are registered for nanoZrO_2-B samples due to the presence of only ZrO_2 clusters organized in such a manner that show relatively narrow pore size distribution with maximum in the range 5–7 nm (Fig. 2). The relatively high specific surface area registered for the mixed ceria-zirconia sample (Table 1) could be assigned to its very narrow pore size distribution (characterized with average pore diameter of about 3.7 nm) due to the presence of interparticle mesoporosity between its very small crystallites (Fig. 2, Table 1). At the same time, the larger crystallites found for nanoZrO_2-A are liable for the presence of interparticle mesoporosity with a much broader pore size distribution that significantly lowers the specific surface area but increases the total pore volume for this sample (Fig. 2, Table 1).

In the FTIR spectra of the three so-prepared nanomaterials, we observed broad bands in the range from 3600 cm^{-1} to 3300 cm^{-1} are assigned to stretching and bending vibrations of the water molecules absorbed on the surface of the carrier. In the spectrum of nanoZrO_2-A, we observed two sharp bands at 745 cm^{-1} and 490 cm^{-1} that are characteristic of monoclinic zirconia and a sharp peak at 570 cm^{-1} that is ascribed to Zr-O vibrations of tetragonal phase. In the spectrum of nanoZrO_2-B, we assigned peaks at 1546 cm^{-1} and 1318 cm^{-1} to the vibrations of Zr-OH bond. Similar bands, attributed to Ce(Zr)-OH bonds at 1540 cm^{-1} and 1330 cm^{-1} have been observed in the spectrum of the mixed zirconia-ceria oxides. However in the spectra of nanoZrO_2-A and nanoZrO_2-CeO_2,

Table 1
Physicochemical characteristics of the newly synthesized zirconium-based supports.

Sample	Metal precursors	BET[a] (m^2/g)	d_{pore}[b] (nm)	V_{tot}[c] (cm^3/g)	D[d] (nm)
nanoZrO_2-A (500 °C)	$ZrCl_4$	54	10.5;15	0.25	15.6 (12.8)[f]
nanoZrO_2-B (100 + 300 °C)	$ZrCl_4$	296	5–7	0.42	1
nanoZrO_2-CeO_2 (300 °C)	$ZrCl_4$ $CeCl_3.7H_2O$ (1:1, moles)	150	3.7	0.14	4.8
nanoCeO_2[f]	$CeCl_3.7H_2O$	58	20	0.27	10

[a] BET specific surface area.
[b] Main pore diameter evaluated from BJH pore size distribution desorption curves (d).
[c] Total pore volume (V_{tot}).
[d] Average particle size calculated with the Scherrer equation (D).
[e] Characteristics of nanoCeO_2 used here are given for comparison.
[f] The values present the size of zirconia crystallites with monoclinic and (tetragonal) structure.

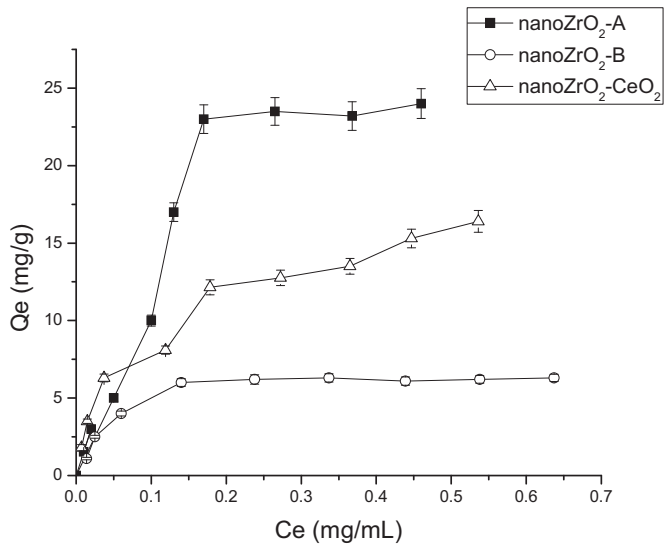

Fig. 3. Langmuir adsorption isotherms for immobilization of lipase from *Candida rugosa* on nanoZrO$_2$-A, nanoZrO$_2$-B, and nanoZrO$_2$-CeO$_2$. Q_e – amount of the protein adsorbed on 1 g carrier. C_e – final concentration of the enzyme loading solutions

the peaks typical for the bonds Zr-O-Zr and Ce-O-Ce or Ce-O-Zr are not observed due to the dilution effect and lack of well-defined phases.

3.2. Immobilization of lipase from Candida rugosa on the nanosized ZrO_2 and ZrO_2-CeO_2

We applied physical adsorption method for immobilization of a lipase from *C. rugosa* on the newly synthesized zirconia (nanoZrO$_2$-A and nanoZrO$_2$-B) and mixed zirconium-cerium oxide (nanoZrO$_2$-CeO$_2$) samples. Regardless of the type of the carrier, the amount of the loaded protein increased with the increase of the protein concentration in the enzyme loading solution until a well-defined plateau was observed which indicated that the adsorption capacity of the carrier for CRL was reached. The experimental data from the adsorption experiments fit to the Langmuir adsorption model (Fig. 3) that implies a monolayer adsorption of the protein molecules on the carrier. This is a condition for catalytically active immobilized biocatalysts to be obtained because lipases are prone to aggregation upon immobilization or in solutions with protein concentration above 1–2 mg/mL [28]. We estimated a saturation value of 6 mg/g for nanoZrO$_2$-CeO$_2$, while for the nanoZrO$_2$-A and nanoZrO$_2$-B it was about 23 mg/g and 12.15 mg/g, respectively. Surprisingly, we succeeded in only 2.75 mg/g protein loading on pure nanosized cerium dioxide with physicochemical characteristics similar to those of nanoZrO$_2$-A (Table 1). Probably, other factors different from particle and pore sizes are also very important for the efficiency of a material as enzyme carrier. The Langmuir constants were obtained from the linearized Langmuir equation (Table 2). Considering the values of K_L/α_L, we can draw a conclusion that the monolayer adsorption capacities of nanoZrO$_2$-CeO$_2$ and nanoZrO$_2$-B were reached and the immobilization procedure can not be further optimized with respect to the enzyme concentration of the loading solutions. In addition, the binding energy between CRL and nanoZrO$_2$-CeO$_2$-B was 4.5-fold higher than that between the same enzyme and nanoZrO$_2$-A (Table 2).

Table 2
Values of the Langmuir constants for adsorption of *Candida rugosa* lipase on the nanosized zirconium-based carriers.

Support	Langmuir constants		
	K_L (mL/g)	α_L (mL/mg)	K_L/α_L (mg/g)
nanoZrO$_2$-A	158.7 ± 4.7	4.3 ± 0.2	37.2 ± 1.5
nanoZrO$_2$-B	294.0 ± 14.7	19.4 ± 0.7	15.5 ± 0.6
nanoZrO$_2$-CeO$_2$	99.9 ± 4.2	10.0 ± 0.4	8.7 ± 0.3

Fitting the adsorption data to Freundlich pattern, we assessed the homogeneity of the support surface from the linearized Freundlich equation [22]. For nanoZrO$_2$-A, nanoZrO$_2$-B, and nanoZrO$_2$-CeO$_2$, the model fit the data with correlation coefficients of 0.95, 0.97 and 0.82, respectively. The homogeneity factor ($1/n$) for the adsorption of CRL on nanoZrO$_2$-A was 0.88, while those for nanoZrO$_2$-B and nanoZrO$_2$-CeO$_2$ were 0.52 and 0.3, respectively. This implies that nanoZrO$_2$-A surface is almost homogeneous and we may assume that lipase molecules have been adsorbed in a monolayer. On the contrary, in the case of the zirconium-based supports with the highest specific area and the smallest sizes (nanoZrO$_2$-B and nanoZrO$_2$-CeO$_2$), the protein molecules were not uniformly distributed on the surface of the carrier and/or multilayer deposition were realized.

The surface area of each carrier which is occupied by the lipase molecules after the immobilization was calculated having in mind that the geometry of native wild-type lipase can be approximated to a sphere with radius of about 3.5 nm [29]. The molecular weight of the *C. rugosa* lipase, as given by the supplier, was about 64 000 Da Estimated roughly, the lipase molecules bounded on nanoZrO$_2$-CeO$_2$ (6 mg/g) require surface area of 8.7 m^2. At the same time the lipase molecules adsorbed on nanoZrO$_2$-A (23 mg/g) and nanoZrO$_2$-B (12.15 mg/g) occupied 17.6 m^2 and 33.2 m^2, respectively. Only 5.8% of nanoZrO$_2$-CeO$_2$ and nanoZrO2-B surface was accessible for the lipase molecules, while the capacity of nanoZrO$_2$-A was much higher and the enzyme occupied about 61% of its surface. Probably large regions of the surface of the two materials, nanoZrO$_2$-CeO$_2$ and nanoZrO$_2$-B, are located in narrow cavities and remained inaccessible for the relatively large protein molecules.

Our results from the adsorption experiments were higher than, or comparable with, those reported in the literature for the CRL on macroporous polymer (15.4 mg/g) [30], glass beads and ion exchange resins (0.4–31.3 mg/g) [31], *etc.* However, the loading capacity of nanoZrO$_2$-A for adsorption of CRL was lower than that achieved on Eupergit (27.8–52.4 mg/g) [32], and γ-Fe$_2$O$_3$ [33].

3.3. Analysis of the changes in the secondary structure of the enzyme upon immobilization by means of Fourier transform infrared spectroscopy

We applied FTIR spectroscopy to assess the effect of the structural characteristics of both nanosized zircon samples on the secondary structure of the immobilized lipase from *C. rugosa*. Using ATR technique, protein absorption bands can be obtained with a good signal-to-noise ratio [34].

We observed in the spectra of the native lipase from *C. rugosa* the absorption bands associated with the stretching vibrations of C–H bonds (between 2850 cm^{-1} and 3000 cm^{-1}) and C=O bonds (1650 cm^{-1}), and the deformation vibrations of C–H bonds (around 1450 cm^{-1}). The three peaks at 1150 cm^{-1}, 1070 cm^{-1} and 1035 cm^{-1} present in the spectra of the native and the immobilized biocatalysts are due to the C-O stretching vibrations of the carbohydrate moieties of the protein molecules.

The FTIR spectra of the native and the immobilized CRL were subjected to curve-fitting analysis in the amide I region (1700–1600 cm^{-1}) in order to determine the relative contribution of each band component (Fig. 1S, Supplementary). The amide I band is due almost entirely to the C=O stretch vibrations (approx. 80%) of the peptide bond and is highly sensitive to small changes in molecular geometry and hydrogen bonding. The positions and the assignments to the secondary structural elements of the components that form the amide I band are given in Table 3. The main

Table 3
Infrared band positions, band areas, and assignments in the amide I spectral region of native and physically adsorbed on nanoZrO2-A and nanoZrO2-B lipase from *Candida rugosa*.

Native lipase from *Candida rugosa*		nanoZrO$_2$-A-CRL		nanoZrO$_2$-B-CRL		Assignment of the bands
υ (cm^{-1})	Band area (%)	υ (cm^{-1})	Band area (%)	υ (cm^{-1})	Band area (%)	
1601	5.67	1606	9.00	1602	10.60	Tyrosine residues
1614	6.69	–	–	–	–	Aggregated strands
1622	7.25	1621	14.60	1619	11.40	
1628	8.99	–	–	–	–	β-Sheets
1636	11.78	1633	9.70	1633	13.80	
1645	11.37	1642	10.70	1645	15.60	Unordered/random coils
1654	15.35	1652	13.80	1653	20.04	α-Helices
1664	11.27	1665	19.90	1669	15.80	β-Turns
1676	12.70	–	–	–	–	
1689	8.92	1683	20.40	1683	7.40	β-Turns/antiparallel β-sheets
–	–	–	–	1694	5.20	Antiparallel β-sheets

secondary structure elements have been observed in the frequency intervals as follows: α-helical structures at 1648–1657 cm^{-1}, organized β-sheet structures at 1620–1640 cm^{-1}, and distorted structures (including β-strands and β-turns) at 1660–1690 cm^{-1}. Comparing the relative peak areas corresponding to the relevant secondary-structural elements, we may conclude that as a whole the secondary-structure of the CRL was preserved upon immobilization on the nanosized zirconia particles. For the immobilized enzymes, we did not observe a significant increase in band areas in the frequency regions corresponding to antiparallel β-sheets (1610–1625 cm^{-1} and 1680–1694 cm^{-1}) in comparison to the free enzyme, which means that the protein molecules were adsorbed in monolayers and no protein aggregates were formed. At the same time in the spectra of the immobilized CRL, we observed up to 1.9 fold increase in the intensity of the peak assigned to the tyrosine residues in comparison with the intensity of the same peak (1601 cm^{-1}) in the spectrum of the native enzyme. Probably due to a conformational change within the protein molecule the tyrosine residues become more exposed to the environment. Possibly upon the immobilization on nanoZrO$_2$-A and nanoZrO$_2$-B the enzyme underwent from "closed" to "open" conformation due to a structural rearrangement typical of the lipase from *C. rugosa* [35].

3.4. Effect of the immobilization on catalytic activity and stability of the lipase from Candida rugosa

We subjected to further biochemical characterization and enantioselectivity studies only the preparation with the higher protein loading, *i.e.* nanoZrO$_2$-A-CRL preparation.

The hydrolytic activity of the immobilized lipase was tested in a reaction of hydrolysis of short-chain fatty-acid triglyceride substrate–tributyrin. NanoZrO$_2$-A-CRL exhibited a specific activity of 120 U/mg prot., while for the soluble CRL it was 95 U/mg prot. The enhanced hydrolytic activity (approx. 25%) of the adsorbed on nanoZrO$_2$-A lipase we attribute to stabilization of the enzyme in its monomeric form and a conformational change within the protein which probably makes the active site of the lipase more accessible to the substrate. The biocatalysts demonstrated relatively good operational stability in several consecutive reaction cycles (Fig. 4). The results are comparable to those obtained for CRL on nanoSnO$_2$ [36]. After the first reaction cycle, usually a sharp decline in enzyme activity is observed which is attributed to desorption of the protein in the water phase. This is the most serious drawback of this easy effective one-step method of immobilization.

The problem with enzyme leaching from the carrier can be overcome when the enzymes are utilized in organic solvents or other non-conventional medium such as ionic liquids, supercritical carbon dioxide, and fluorous solvents [37]. Furthermore, the natural substrates of the lipases are highly hydrophobic and the use of solvents may increase their solubility and that result in increase of their effective substrate concentration. In addition the stability of lipases in non-aqueous media may promote their new applications.

Table 4
Stability of nanoZrO$_2$-A-CRL in organic solvents.

Solvent	log *P* [38]	Relative stability (%)	
		Native lipase	nanoZrO$_2$-CRL
Phosphate buffer pH 7.0	–	100.0 ± 2.8	100.0 ± 3.1
Methanol	−0.76	3.0 ± 0.1	15.1 ± 0.5
Ethanol	−0.24	5.1 ± 0.2	28.3 ± 1.3
Acetone	0.23	7.2 ± 0.2	35.7 ± 1.7
Diethyl ether	0.77	60.4 ± 2.4	85.4 ± 2.4
Methyl tert-butyl ether	0.94	68.3 ± 3.2	88.7 ± 2.8
Toluene	2.50	55.0 ± 1.8	68.3 ± 2.0
Hexane	3.50	90.8 ± 4.1	130.6 ± 3.1
N-Heptane	4.00	90.3 ± 3.5	115.8 ± 3.1
Isooctane	4.50	78.4 ± 3.1	95.7 ± 2.6

Reaction conditions: 0.1 mL tributyrin (mol), 0.1 mL gum arabica (5 mg/mL), 5 mL phosphate buffer (pH 7.0, 50 mM), 5 mg nanoZrO$_2$-A-CRL,40 °C (or 10 μL soluble enzyme), 30 min, 200 rpm stirring. Biocatalysts were treated with solvent for 1 h prior to use.

We tested the activity of the nanoZrO$_2$-A-CRL in various organic solvents with polarity (log *P*) ranging from −0.76 to +4.5. (*P* is octanol–water partition coefficient) [38]. The results are discussed with respect to the behaviour of the soluble enzyme in the same solvents (Table 4). The stability in hydrophobic solvents is not surprising for the lipases. It is the best explained with the structural and the mechanistic peculiarities typical of this group of enzymes. Depending on their environment, the lipase molecules can be found in two conformations – "open" (active) and "closed" (inactive) which are due to structural rearrangements similar to those induced by substrates. Many lipases are activated in a non-polar solvent which is a result of substantial conformational change

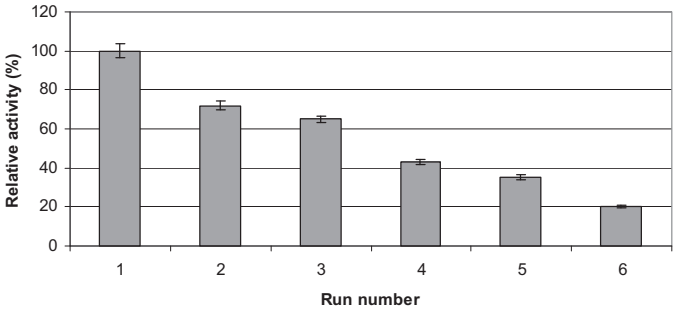

Fig. 4. Stability of nanoZrO$_2$-A-CRL in several consecutive cycles. Reaction conditions: 0.1 mL tributyrin (moles), 0.1 mL gum arabica (5 mg/mL), 5 mL phosphate buffer (pH 7.0, 50 mM), 40 °C, 30 min, 200 rpm stirring.

of the protein molecule induced upon contact with a hydrophobic surface (substrate, hydrophobic carriers or solvents). As a result the active site of the enzyme becomes accessible for the substrate.

However, similarly to most of the enzymes, lipases are not active in presence of polar solvents. Solvents with log $P < 2$ are considered hydrophilic, they tend to strip away the water molecules from the protein surface that are responsible for maintaining protein structure, thus they have destabilizing effect on the enzyme [39]. Stabilization of lipases in such solvents is a challenge and is of importance in many aspects. For example, recently one of the most attractive applications of lipases has been in the biodiesel production. The fuel can be obtained in lipase-catalyzed alcoholysis of natural plant oils, and therefore the enzymes should be stable and active in presence of short-chain alcohols which are one of the reagents. We observed an enhanced stability of the immobilized CRL in all polar solvents (Table 4). It is worth mentioning the remarkable stability of nanoZrO_2-A-CRL in 100% acetone which is 5-fold higher than that of the native enzyme. One possible explanation is that porous carriers are able to preserve the favourable microenvironment (humidity) around the enzyme and thus to protect immobilized enzymes from dehydration.

Along with solvent stability, thermal stability is another important characteristic of immobilized biocatalysts. The operation at higher temperatures ensures better solubility and homogenization of the highly viscous fats and plant oils which are the natural lipase substrates, minimizes the risk of bacterial contamination of the products and enhances the reaction rate. The native CRL operates at 37 °C and it is easily inactivated with temperature increase. Expectedly, the immobilization enhanced the thermal stability of CRL (Fig. 5). We estimated that the half-life ($t_{1/2}$) of the immobilized on nanoZrO_2-A lipase was 73 min at 55 °C (pH 7.0) while soluble enzyme was much faster inactivated at the same reaction condition ($t_{1/2}$ 5.3 min).

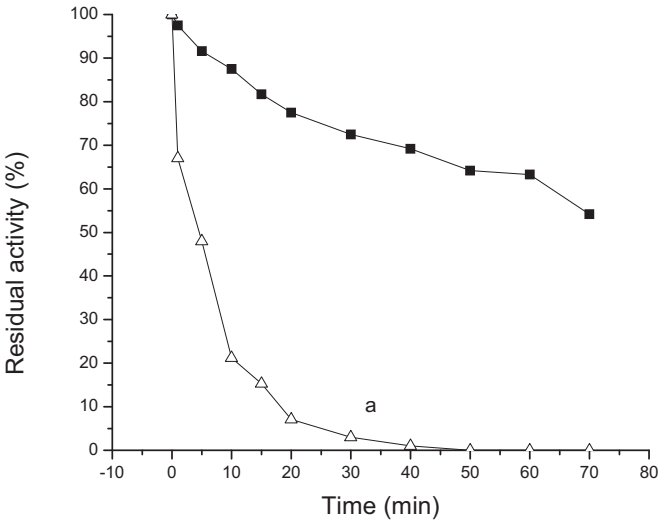

Fig. 5. Thermal stability of the native (a) and immobilized on nanoZrO_2-A (b) lipase from *Candida rugosa* at 55 °C.

3.5. Effect of the immobilization on enantioselectivity of the lipase from Candida rugosa

(−)-Menthol is a high-value substance which is used in drug delivery emulsions due to its properties to enhance skin permeation of some drugs [40]. It can be isolated from the peppermint together with eight other isomers, however, the typical refreshing or cooling effect is limited only to (−)-menthol. We chose as acylating reagents lauric acid and its methyl ester taking into account the fatty acid-chain length specificity of CRL. It is known that organic acid anhydrides and vinyl esters are highly reactive. However, the anhydrides of long-chain fatty acids are very expensive and heat labile, and on the other hand, formaldehyde, a toxic by-product, can be formed when vinyl esters are used. The detailed evaluation of the effect of acyl donor and solvent on the reaction was carried out using the parameters extent of conversion (c), enantiomeric excess of the product (e.e.(P_-)) and enantiomeric ratio (E) (Table 5). The two enzymes, native and immobilized, exhibited good selectivity towards the (−)-menthol as a substrate. Nano-ZrO_2-A-CRL exhibited higher esterification activity than the native enzyme which probably is due to the protein stabilization upon immobilization. For nanoZrO_2-A-CRL-catalyzed acidolysis the degree of conversion of (±)-menthol was comparable in i-octane and hexane and was up to two-fold higher than in methyl tert-butyl ether. The solvent did not influence the reaction rate when native enzyme was used as catalyst. Not surprisingly, methyl laurate facilitates the acylation up to 1.3-fold (hexane, nanoZrO_2-A-CRL), however, less pure products were synthesized.

The effect of the temperature on the enantioselectivity was tested in the temperature range from 20 °C to 40 °C (Fig. 6). The highest yields were obtained at 40 °C, and the conversion of (±)-menthol exceeded 50% with nanoZrO_2-A-CRL. However, the increase of the reaction temperature with 20 °C resulted in 2.5-fold decrease in selectivity of the native enzyme, while for nanoZrO_2-A-CRL the reduction was about 4-fold. Lowering the temperature in the lipase-catalyzed resolution usually enhances enantioselectivity. The phenomenon does not come from the temperature-induced conformational change of lipase, but the explanation can be found on the basis of the physical organic chemistry. In general, enantioselectivity, enantiomeric ratio, in a kinetic controlled

Table 5
Effect of the solvent and the acyl donor on the enantioselectivity of the lipase from *Candida rugosa*.

Enzyme	Solvent	Acyl donor	(±)-Menthol conversion	ee (P_-), %	Enaniomeric ratio (E)
Native lipase from *C. rugosa*	MTBE	Lauric acid	11.4	93.0	31
		Methyl laurate	15.8	90.1	22.4
	Hexane	Lauric acid	17.7	94.3	41.3
		Methyl laurate	20.3	93.6	38.3
	i-Octane	Lauric acid	17.3	89.3	21.3
		Methyl laurate	20.4	84.5	14.7
nanoZrO_2-A-CRL	MTBE	Lauric acid	31.0	95.8	71
		Methyl laurate	38.4	88.0	26
	Hexane	Lauric acid	43.0	97.0	144
		Methyl laurate	58.3	60.0	10
	i-Octane	Lauric acid	48.0	95.3	121
		Methyl laurate	57.5	68.1	17

Reaction conditions: (±)-menthol (4 mmol), acylating reagent (4 mmol), immobilized lipase (5 U), 25 °C, 200 rpm, 24 h, a_w = 0.33.
MTBE – methyl *tert*-butyl ether.

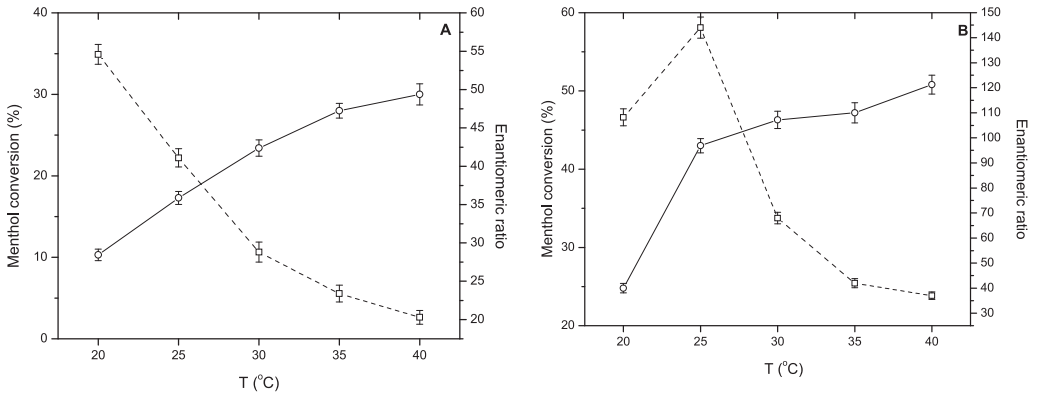

Fig. 6. Effect of temperature on activity and enantioselectivity of the native (A) and immobilized on nanoZrO$_2$-A-CRL (B) lipase from *Candida rugosa* in the reaction of acylation of (±)-menthol. Reaction conditions: (±)-menthol (4 mmol), lauric acid (4 mmol), immobilized lipase (5 U), 20–40 °C, 200 rpm, 24 h, hexane, a_w = 0.33. Dependences of menthol conversion (%) *vs T* °C are presented with straight lines. Dependences of enantiomeric ratio *vs T* °C are presented with dotted lines.

reaction is determined by the ratio of the rates of the two enantiomers [41].

We obtained a degree of conversion of (±)-menthol comparable to the reported in the literature for other immobilized lipases from *C. rugosa*. In some reactions we obtained products with higher purity. Under optimal reaction conditions (25 C, hexane, 24 h), nanoZrO$_2$-A-CRL exhibited higher enantioselectivity than that reported by Wang et al. for CRL on DEAE-Sephadex A25 (e.e. 95%, *E* 87.7) [42] as well as those reported by Yuan et al. for the native CRL in hexane (e.e. 88%, *E* 31.9%) [43].

4. Conclusions

Zirconia or zirconia-based materials are attractive enzyme supports with great potential. For the three tested materials, we estimated that the loading capacity of the carriers seems to depend not only on the physicochemical properties of the material but also on their structural characteristics. For example, we achieved up to 9-fold higher protein loading on nanoZrO$_2$-A in comparison with those on nanoCeO$_2$ although the two materials have similar specific surface area, particle and pore sizes. We found that a lipase from *C. rugosa* physically adsorbed on nanoZrO$_2$-A exhibited an improved thermal and solvent stability as well as enantioselectivity in comparison to the soluble enzyme. NanoZrO$_2$-A seems to be a good material able to stabilize efficiently large protein molecules like those of lipase from *C. rugosa*, thus further experiments with stabilization of other proteins and/or enzymes on nanoZrO$_2$-A worth is carried out.

Acknowledgements

The authors thank the Ministry of Education, Youth and Science of Bulgaria (Project “Science and business” BG051PO001-3.3.05-0001) for the financial support.

Appendix A. Supplementary data

Supplementary data associated with this article can be found, in the online version, at http://dx.doi.org/10.1016/j.molcatb.2014.06.012.

References

[1] M. Kapoor, M. Gupta, Process Biochem. 47 (2012) 555–569.
[2] U. Bornscheuer, FEMS Microbiol. Rev. 26 (2002) 73–81.
[3] R. Schmid, R. Verger, Angew. Chem. Int. Ed. 37 (1998) 1608–1633.
[4] P. Reis, K. Holmberg, H. Watzke, M.E. Leser, R. Miller, Adv. Colloid Interface Sci. 147–148 (2009) 237–250.
[5] J. Palomo, R. Segura, G. Fernandez-Lorente, M. Pernas, M. Rua, J. Guisan, R. Fernandez-Lafuente, Biotechnol. Prog. 20 (2004) 630–635.
[6] M. Bellusci, I. Francolini, A. Martinelli, L. D'Ilario, A. Piozzi, Biomacromolecules 13 (2012) 805–813.
[7] A. Bastida, P. Sabuquillo, P. Armisen, R. Fernandez-Lafuente, J. Huguet, J. Guisan, Biotechnol. Bioeng. (1998) 486–493.
[8] A. Houde, A. Kademi, D. Leblanc, Appl. Biochem. Biotechnol. 118 (2004) 155–170.
[9] C. Garcia-Galan, A. Berenguer-Murcia, R. Fernandez-Lafuente, R. Rodrigues, Adv. Synth. Catal. 353 (2011) 2885–2904.
[10] J. Ge, Ch. Yang, J. Zhu, D. Lu, Z. Liu, Top Catal. 55 (2012) 1070–1080.
[11] M. Lal Verma, C. Barrow, M. Puri, Appl. Microbiol. Biotechnol. 97 (2013) 23–39.
[12] E. Cipolatti, M. Silva, M. Klein, V. Feddern, M. Feltes, J. Oliveira, J. Ninow, D. de Oliveira, J. Mol. Catal. B: Enzym. 99 (2014) 56–67.
[13] M. Hartmann, X. Kostov, Chem. Soc. Rev. 42 (2013) 6277–6289.
[14] R. Reshmi, G. Sanjay, S. Sugunan, Catal. Commun. 8 (2007) 393–399.
[15] F. Bellezza, A. Cipiciani, M.A. Quotadamo, Langmuir 21 (2005) 11099–11104.
[16] F. Bellezza, A. Cipiciani, U. Costantino, J. Mol. Catal. B: Enzym. 26 (2003) 47–56.
[17] J. Vakhlu, A. Kour, Electron. J. Biotechnol. 9 (2006) 69–85.
[18] F. Hasan, A. Shah, A. Hameed, Enzyme Microb. Technol. 39 (2006) 235–251.
[19] T. Tsoncheva, L. Ivanova, D. Paneva, I. Mitov, C. Minchev, M. Fröba, Micropor. Mesopor. Mater. 120 (2009) 389–396.
[20] C. Hammond, The diffraction of X-rays, in: The Basics of Crystallography and Diffraction, Oxford Science Publications, New York, 2001, pp. 203–242.
[21] O.H. Lowry, N.J. Rosebrough, A.L. Farr, R.J. Randall, J. Biol. Chem. 193 (1951) 265–275.
[22] B. Al-Duri, Y.P. Yong, J. Mol. Catal. B: Enzym. 3 (1997) 177–188.
[23] A. Natalello, D. Ami, S. Brocca, M. Lotti, S.M. Doglia, Biochem. J. 385 (2005) 511–517.
[24] F. Secundo, G. Carrea, Biotechnol. Bioeng. 92 (2005) 438–446.
[25] G. Sathya Narayana Naidu, T. Panda, Biochem. Eng. J. 16 (2003) 57–67.
[26] P. Halling, Biotechnol. Tech. 6 (1992) 271–276.
[27] A. Straathof, J. Jongejan, Enzyme Microb. Tech. 21 (1997) 559–571.
[28] M.L. Foresti, A. Errazu, M.L. Ferreira, Biochem. Eng. J. 25 (2005) 69–77.
[29] P. Grochulski, Y. Li, J.D. Schrag, F. Bouthillier, P. Smith, D. Harrison, B. Rubin, M. Cygler, J. Biol. Chem. 268 (1993) 12843–12847.
[30] L. Mojovic, Z. Knezevic, R. Popadic, S. Jovanovic, Appl. Microbiol. Biotechnol. 50 (1998) 676–681.
[31] A. Bodalo, J. Bastida, M.F. Maximo, M.C. Montiel, M. Gomez, M.D. Murcia, Biochem. Eng. J. 39 (2008) 450–456.
[32] Z. Knezevic, N. Milosavic, D. Bezbradica, Z. Jakovljevic, R. Prodanovic, Biochem. Eng. J. 30 (2006) 269–278.
[33] A. Dyal, K. Loos, M. Noto, S. Chang, Ch. Spagnoli, K. Shafi, U. Abraham, M. Cowman, R. Gross, J. Am. Chem. Soc. 125 (2003) 1684–1685.
[34] A. Barth, Biochim. Biophys. Acta 1767 (2007) 1073–1101.
[35] P. Grochulski, Y. Li, J. Schrag, M. Cygler, Prot. Sci. 3 (1994) 82–92.
[36] M. Guncheva, M. Dimitrov, D. Zhiryakova, Process Biochem. 46 (2011) 2170–2177.
[37] P. Lozano, Green Chem. 12 (2010) 555–569.
[38] C. Laane, S. Boeren, K. Vos, C. Beeger, Biotechnol. Bioeng. 30 (1987) 81–87.
[39] A. Klibanov, Trends Biochem. Sci. 14 (1989) 141–149.
[40] A. Kogan, N. Garti, Adv. Colloid Interface Sci. 123–126 (2006) 369–385.
[41] P. Overbeeke, J. Ohosson, K. Hult, J. Jongejan, J. Duine, Biocatal. Biotransform. 17 (1999) 61–67.
[42] D. Wang, A. Nag, G. Lee, J. Shaw, J. Agric. Food Chem. 50 (2002) 262–265.
[43] Y. Yuan, S. Bai, Y. Sun, Food Chem. 97 (2006) 324–330.